

High Spectral Resolution Plasmonic Color Filters with Subwavelength Dimensions

Dagny Fleischman, Katherine T. Fountaine, Colton R Bukowsky,
Giulia Tagliabue, Luke A. Sweatlock, and Harry A Atwater

ACS Photonics, **Just Accepted Manuscript** • DOI: 10.1021/acsp Photonics.8b01634 • Publication Date (Web): 02 Jan 2019

Downloaded from <http://pubs.acs.org> on January 3, 2019

Just Accepted

“Just Accepted” manuscripts have been peer-reviewed and accepted for publication. They are posted online prior to technical editing, formatting for publication and author proofing. The American Chemical Society provides “Just Accepted” as a service to the research community to expedite the dissemination of scientific material as soon as possible after acceptance. “Just Accepted” manuscripts appear in full in PDF format accompanied by an HTML abstract. “Just Accepted” manuscripts have been fully peer reviewed, but should not be considered the official version of record. They are citable by the Digital Object Identifier (DOI®). “Just Accepted” is an optional service offered to authors. Therefore, the “Just Accepted” Web site may not include all articles that will be published in the journal. After a manuscript is technically edited and formatted, it will be removed from the “Just Accepted” Web site and published as an ASAP article. Note that technical editing may introduce minor changes to the manuscript text and/or graphics which could affect content, and all legal disclaimers and ethical guidelines that apply to the journal pertain. ACS cannot be held responsible for errors or consequences arising from the use of information contained in these “Just Accepted” manuscripts.

High Spectral Resolution Plasmonic Color Filters with Subwavelength Dimensions

Dagny Fleischman¹, Katherine T. Fountaine², Colton R. Bukowsky¹, Giulia Tagliabue¹, Luke A. Sweatlock², and Harry A. Atwater¹

1. Thomas J. Watson Laboratories of Applied Physics, California Institute of Technology, Pasadena, CA 91125
2. Northrop Grumman NG Next, One Space Park, Redondo Beach, CA 90250, USA

Abstract: Rapid advances in image sensor technology have generated a mismatch between the small size of image sensor pixels and the achievable filter spectral resolution. This mismatch has prevented the realization of chip-based image sensors with simultaneously high spatial and spectral resolution. We report here a concept that overcomes this tradeoff, enabling high spectral resolution (transmission FWHM < 31 nm) filters with subwavelength dimensions operating at optical and near infrared wavelengths. An inverse design methodology was used to realize a new type of plasmonic cavity that efficiently couples an in-plane Fabry-Perot resonator to a single plasmonic slit that supports surface plasmon polaritons. This design principle, combined with a new metal imprinting method that yields metallic nanostructures with both top and bottom surfaces that are extremely smooth, enabled demonstration of high spectral resolution transmission filters with smaller area than any previously reported.

Keywords: nanophotonics, plasmonics, multi-mode structures, nanostructures, multispectral filtering, inverse design

The concept of dimensional scaling has been a cornerstone of solid-state integrated device technology over the past 50 years, fueling ‘Moore’s law’ performance advances in silicon integrated circuits¹, magnetic memories², optical fiber data transmission³, among others. Dimensional scaling of pixel size from over 10 μm to as small as 1.1 μm in CMOS digital image sensor arrays over the last decade has led to greatly increased electronic image resolution, accomplished by coupling an objective lens to a focal plane area populated by an ever-increasing number of pixels at constant array size⁴. These image sensors utilize filters composed of dye-doped polymers that allow them to transmit incident light over red, green, and blue ranges of the visible spectrum to form a color image. Such dye-based color filters typically do not allow for high spectral resolution but are adequate for 3-color imaging. Many alternative color filter

1
2
3 concepts based on resonances in nanophotonic structures have been explored in attempt to improve
4 upon the transmission efficiency, spectral resolution and spatial resolution of dye based color
5 filters, which suffer from issues with optical cross-talk at small length scales and degradation under
6 UV radiation³. Successful demonstrations of hole and slit array filters have relied on short range
7 order, achieving footprints as small as 1 μm ^{4,5}. However, these small footprint filters possess
8 relatively large transmission bandwidths, on the order of 100-150 nm, sufficient for 3-color
9 imaging but not for multispectral or hyperspectral imaging. However, if filters could be realized
10 that feature transmission bandwidths less than 30 nm, rather than filtering just three colors,
11 imaging systems could be designed to spectrally separate the visible and near-infrared spectrum
12 into 20 colors or more, enabling acquisition and construction of an optical spectrum at every pixel
13 in an image^{6,7}. This type of data collection, termed hyperspectral imaging, provides image sensors
14 with the ability to perform spectroscopy at every pixel in an image. The ability to perform
15 multispectral and hyperspectral imaging functions using a compact CMOS image sensor without
16 any moving parts would have far-reaching impacts in fields as disparate as healthcare, food quality
17 control, and space exploration⁸⁻¹⁰
18
19
20
21
22
23
24
25
26
27
28
29

30 While there have been demonstrations of nanophotonic color filter architectures capable
31 of producing narrow transmission bandwidths, these filters are large, because they rely on medium-
32 to-long range periodic effects to produce their narrow spectral features¹¹⁻¹⁴. Guided-mode
33 resonance filters (GMRs) utilize a transmissive waveguide grating to produce a resonant
34 response¹². The resolving power ($\lambda/\Delta\lambda$) of the transmission band is directly related to the number
35 of periods¹⁵. To achieve a narrow spectral resonance, GMR filters require approximately 50 lattice
36 periods, which gives them a spatial footprint on the 10s of microns at optical wavelengths, making
37 them far too large to serve as color filters in CMOS image sensors¹⁵.
38
39
40
41
42
43
44
45
46
47
48
49
50
51
52
53
54
55
56
57
58
59
60

This relationship between quality factor and lattice periodicity is not particular to GMR filters but is related to the spatial-spectral transform relations of periodically-structured media. In general, as the number of periods (N) in a filter increases, so does the spectral resolving power. As shown in Figure 1 for experimental results, hole array filters, single film slit array filters, and single film Fabry-Perot resonant filters can all exhibit relatively small footprints, but their experimental spectral transmittances are broad, and color separation is limited to 3 or 4 spectral bands^{4,5,16,17}. Multilayer slot mode plasmonic color filters introduced an additional dimension of periodicity, which allowed for a narrower response, but the footprint of these filters, while smaller than GMR filters, is still too large for the smallest pixel image sensor applications¹¹.

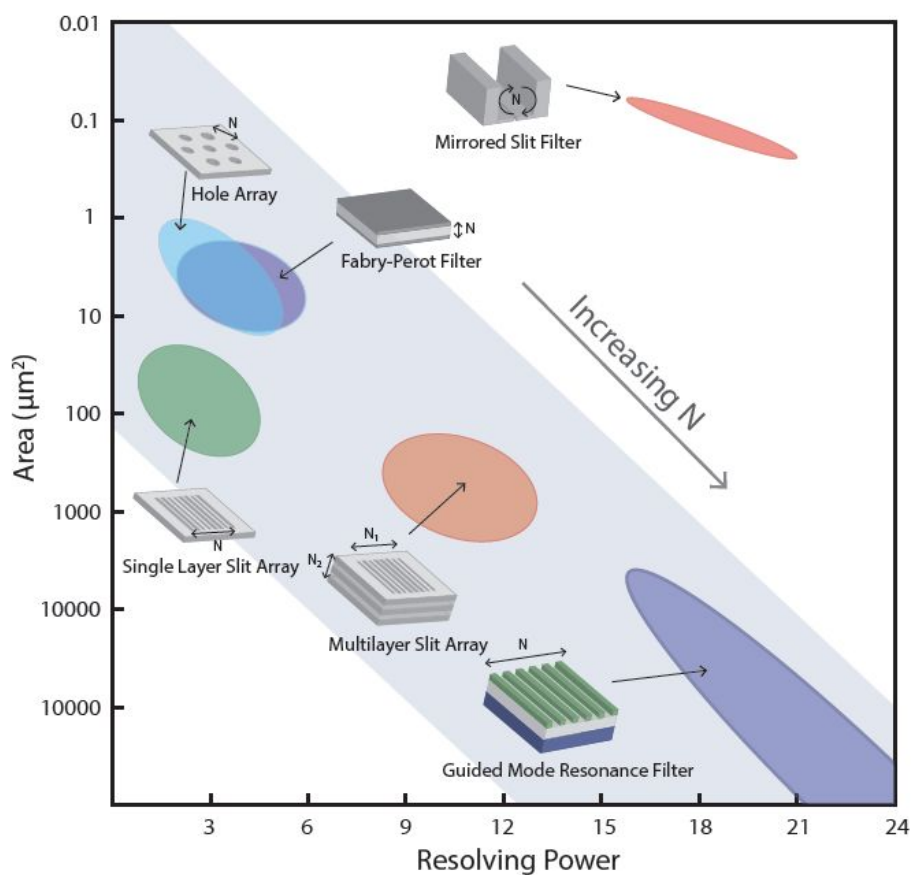


Figure 1 The relationship between the spatial area of a filter and its resolving factor ($\lambda/\Delta\lambda$) for transmission color filters in the visible part of the spectrum. The general trend is shown in the grey region, where smaller footprint filters possess large spectral features and larger footprint filters possess smaller spectral features. This relationship is dictated by N , the number of periods contained within the filter. This relationship is broken by the mirrored slit filter (small red oval), because the mirrors create an effectively large number of periods within a very confined space.

1
2
3 While this relationship is shown for spatial area in Figure 1, this trend also holds for the volume
4 of color filters. In general, the larger the volume of the filter, the narrower the transmission
5 response, as shown by the narrowing of the spectral response of Bragg gratings as their number of
6 periods increases¹⁸.
7
8
9

10
11 Reflective boundaries at the edges of a smaller footprint all-dielectric microwave GMR
12 filters have been used to create a synthetic long range order in smaller footprint structures¹⁹. In
13 this paper, we use highly reflective metal boundaries on a single plasmonic slit to break the
14 relationship illustrated in Figure 1 between footprint and periodicity. The metal mirrors in the
15 mirrored filter impose effective periodic boundary conditions on the transmission slit, that in the
16 lossless limit would introduce infinite periodicity into a small footprint structure. These filters are
17 simultaneously smaller than any color filter described in the literature and possess a resolving
18 power on par with the highest performing nanophotonic visible light color filters that benefit from
19 long range order effects.
20
21
22
23
24
25
26

27
28 The mirrored filters possess highly coupled parameters that can be used to control the
29 filters performance. The schematic shown in Figure 2(a) shows the main parameters considered
30 during the optimization of these filters: mirror height, mirror spacing, slit width, film thickness,
31 and oxide thickness. The general design of the mirrored color filter takes advantage of multiple
32 resonances within the structure. A gap mode, shown in Figure 2(b), is supported in the deeply
33 subwavelength slit that penetrates the thin film. Figure 2(c) shows a cavity mode supported by
34 two vertical mirrors, where the available cavity modes are dictated by the mirror spacing, mirror
35 height, and oxide thickness. These modes can be used to produce narrowband spectral responses
36 in Fabry-Perot filters¹⁴. The thin film also supports surface plasmon polariton modes (SPPs) on
37 its top and bottom surfaces. A top surface SPP mode is shown in Figure 2(d). SPP modes have
38 been used to produce transmission color filtering when incorporated into a grating structure. In
39 addition to these three types of modes, there are numerous other modes supported by this structure.
40 However, the transmission filters that exhibit high spectral resolution are characterized by coupling
41 of these three modal types to achieve narrowband filter performance. By optimizing a structure to
42 be resonant at specific wavelengths, it is possible to produce narrow-bandwidth transmission color
43 filtering.
44
45
46
47
48
49
50
51
52
53
54
55
56
57
58
59
60

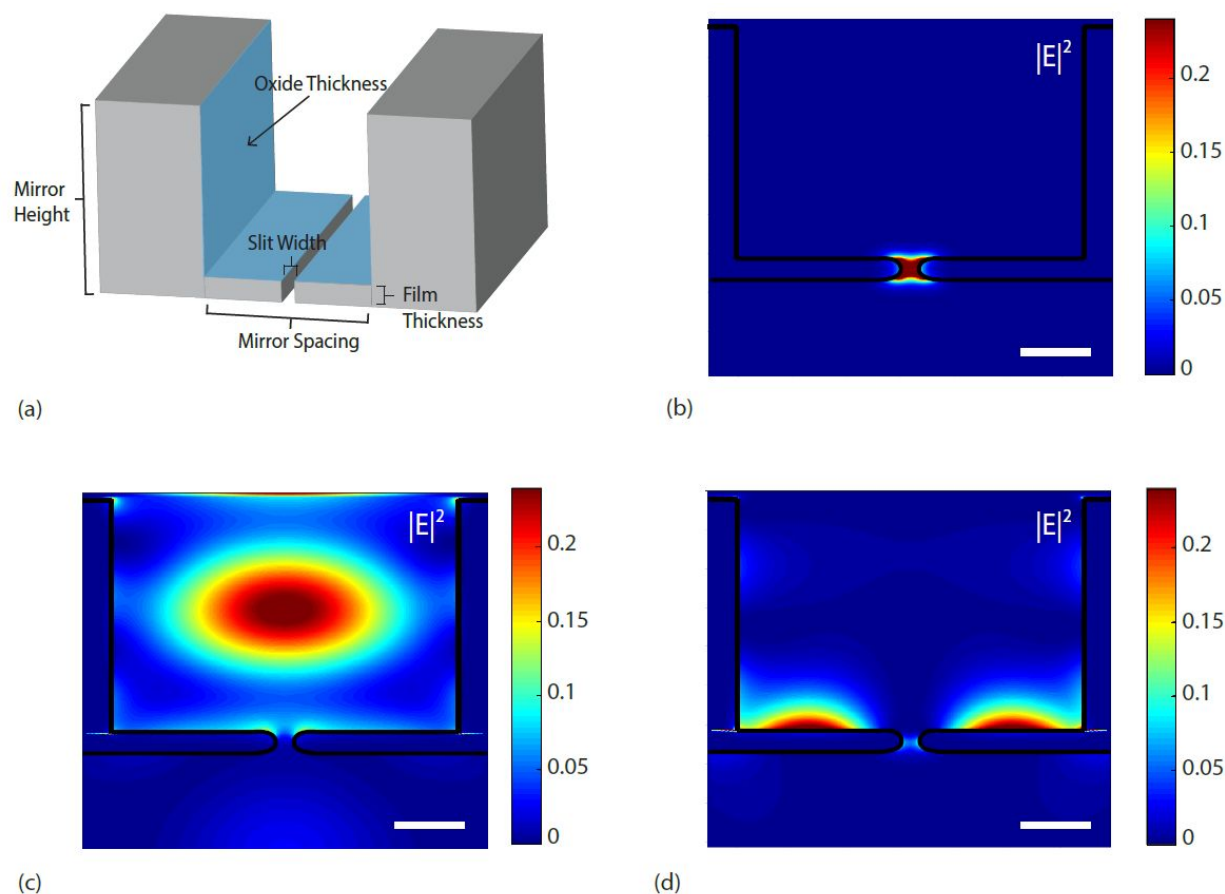


Figure 2 (a) Schematic of the narrowband transmission filter showing the main structure parameters: film thickness, mirror height, mirror spacing, slit width, and oxide thickness (shown in blue). The optimal filter was found to possess a film thickness of 48 nm, mirror height of 598 nm, slit width of 31 nm, an oxide thickness of 1 nm for a variety of mirror spacings (b) Electric field intensity profile for sample eigenmode solutions for a mirrored slit filter illustrating the gap mode within the slit in the thin film with behavior controlled by the slit width and film thickness (c) Electric field intensity profile for the cavity mode contained between the two mirrors with behavior controlled by the mirror height, mirror spacing, and oxide thickness (d) Electric field intensity profile for surface plasmon polariton mode supported on the surface of the thin film with behavior controlled by the film thickness, oxide thickness, mirror spacing, and slit width. The scale bar on (b)-(d) is 100 nm.

As demonstrated by Supplemental Figures 1 and 2, two of the features most responsible for the narrowband transmission response are the efficiency of the gap mode and the thickness of the thin film spanning the distance between the two reflective mirrors. The coupling efficiency of the gap mode dictates the overall transmission intensity of the filter. Without the ability to efficiently couple into the gap mode excitation, the overall transmission response is low. The

1
2
3 linewidth of the transmission response was shown to strongly depend on the thickness of the metal
4 film. When the metal film is thin, excited modes can couple across it, which leads to a much
5 narrower transmission response, even when all other physical parameters are held fixed. While
6 these two aspects of the filter play a large role in the transmission response, changes to any of the
7 filter dimensions were found to affect the coupling of the excited modes and the resulting
8 transmission of the filters. The height and spacing of the mirrors, the thickness of the thin film,
9 the slit width, the high index oxide coating thickness, and the materials chosen as the metal and
10 dielectric components all affect the filter transmission efficiency and linewidth.
11
12
13
14
15
16
17

18 Even for a fixed set of chosen dielectric and metallic materials, the number of parameters
19 is too high and their relationships too complex to effectively optimize filter transmission efficiency
20 and linewidth by heuristic analysis and inductive physical reasoning alone. To ensure a strong
21 candidate filter was identified, a numerical optimization method was used to design the champion
22 filter fabricated in this study. The Nonlinear Mesh Adaptive Direct Search algorithm (NOMAD)
23 was selected to optimize this structure because of its computational efficiency and the ability to
24 use surrogate functions^{20–22}. After the surrogate function is approximated, this hybrid global and
25 local search method alternates between searching and polling on a mesh of points within the
26 parameter space. The resolution of this mesh is adjusted by the algorithm to allow for addressing
27 both coarse and fine probing within the parameter space, which facilitates both efficiently finding
28 the optimum value and preventing the algorithm from getting trapped in local minima. The figure
29 of merit (FOM) used for spectrally narrowband transmission filter design accounts for the spectral
30 constraints on the filter,
31
32
33
34
35
36
37
38
39
40

$$41 \quad FOM = (\text{deltawav}/c.\text{wav}) + (c.\text{peak}/\text{peak}) + (\text{noise}/c.\text{noise}) + (FWHM/c.FWHM)$$

42
43

44 This relation seeks to maximize the intensity of a single peak at the desired wavelength (*peak*)
45 while minimizing both the FWHM (*FWHM*) of that peak and the intensity of any additional peaks
46 (*noise*). It also seeks to shift the maximum intensity of the peak to the intended transmission band
47 of the filter (*deltawav*). Each term has a weighting factor (*c.wav*, *c.peak*, *c.noise*, and *c.FWHM*)
48 that can be used to enhance or suppress the effect of a given term in the FOM. These weighting
49 factors were varied during the study, but the champion filter identified had the following weighting
50 factors: *c.wav* = 0.1, *c.peak* = 1, *c.noise* = 5, *c.FWHM* = 5 to yield a filter with *deltawav* = 0.5 nm,
51
52
53
54
55
56
57
58
59
60

peak = 25.3%, noise = 49, and FWHM = 15 nm. The optimization produced a spread of FOMs, starting as high as 330 and reaching as low as 16.7. To develop the champion filter shown in Figure 2(a), five parameters were varied: mirror height, mirror spacing, slit width, film thickness, and the thickness of a HfO_2 layer coating the metal filter. We also found that while additional slits can be used to improve the overall transmission intensity of the color filter, these additional slits increase the footprint of the filter, so the number of slits was fixed to one. The spacing between the mirrors of this optimized filter is 618 nm. The fields of the modes supported by the structure were calculated to penetrate 46 nm into each mirror, leading to a full footprint of 710 nm.

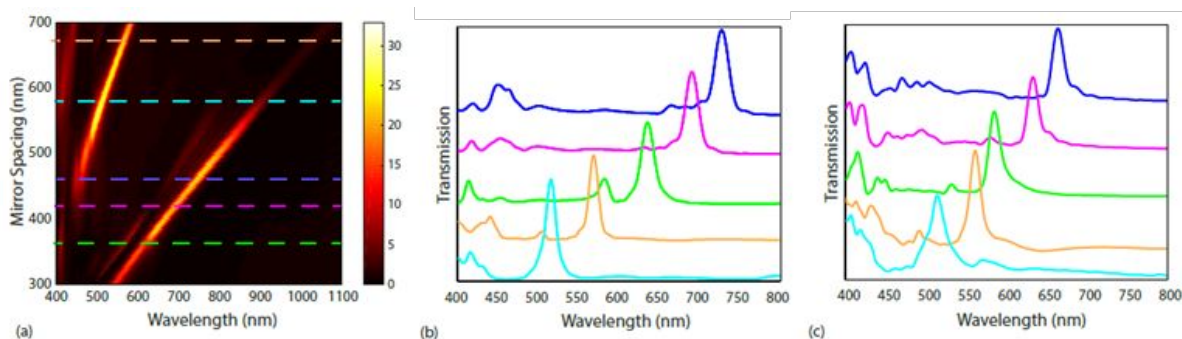


Figure 3 (a) A superposition of transmission plots illustrating the effect of mirror spacing on transmission peak position for 2D linear filters. There are two active mode orders in the visible spectrum, the shorter wavelength transmission band corresponds to the lowest order cavity mode and the longer wavelength band corresponds to the first higher order cavity mode (b) The simulated transmission response of the optimized 2D linear filter for a few mirrored filters spanning the visible part of the spectrum (c) The simulated transmission response of a few 3D square filters with the same mirror spacings as the filters shown in (b).

The transmission peak of the optimized filter can be shifted across the spectrum by changing the position of the mirrors. Figure 3(a) shows a superposition of transmission curves for filters with different mirror spacing for linear filters in a 2D simulation environment. The superposition plot indicates there are two active transmission bands in the visible part of the spectrum, one corresponding to shorter wavelengths and one corresponding to longer wavelengths. The FWHM of these optimized filters varied from 14 – 26 nm across the visible spectrum. The FWHM of these filters is in large part dictated by the optical loss present in Ag. We also investigated filter design for the same structures under the assumption of a metal that acts as a perfect electric conductor. In these lossless structures, filter structures were found to exhibit FWHM values as low as 7 nm.

1
2
3 We explored the mode orders associated with these transmission bands using an
4 eigenmode solver, and the results indicated that the shorter wavelength band is due to the lowest
5 order cavity mode, while the longer wavelength transmission arises from the second-order cavity
6 mode. To further illustrate the transmission response, Figure 3(b) shows a few representative
7 transmission spectra for linear filters with a single slit. Between the two different transmission
8 bands these filters possess narrowband transmission behavior across most of the visible and part
9 of the near IR portions of the spectrum. To demonstrate that the principles at work in the
10 performance of the two-dimensional filters also apply for three-dimensional filters comprised of
11 two crossed slits instead of a linear slit, three-dimensional simulations were performed for the
12 same geometrical parameters and materials used in the two-dimensional filters. The results of
13 these simulations are shown in Figure 3(c) and illustrate that despite the submicron areas of three-
14 dimensional filters, the resonant modes excited in the three-dimensional structures are similar to
15 those seen in two-dimensional filters.
16
17
18
19
20
21
22
23
24
25

26 The sidewalls of the mirrors were found to strongly affect filter transmittance. Slight
27 changes to the mirror spacing or sidewall taper can dramatically change filter performance. To
28 closely control the quality of the mirrors, the filters were fabricated using a novel metal imprinting
29 method, illustrated in Figures 4(a) and 4(b). This method, described in the Supplemental Section,
30 produces metallic nanostructures with extremely smooth metal surfaces on both sides. While
31 template stripping methods are able to produce very smooth surface on one side of the metallic
32 structure²³, the other surface has a roughness defined by metallic grain growth during vapor
33 deposition. By contrast, our metal imprinting yields equivalently smooth surfaces on both sides
34 which is critical to narrowband filter performance. The imprinting method was also found to yield
35 straighter, smoother and more vertically-oriented metallic sidewalls than is achievable via either
36 metal etching or lift-off processing.
37
38
39
40
41
42
43
44
45
46
47
48
49
50
51
52
53
54
55
56
57
58
59
60

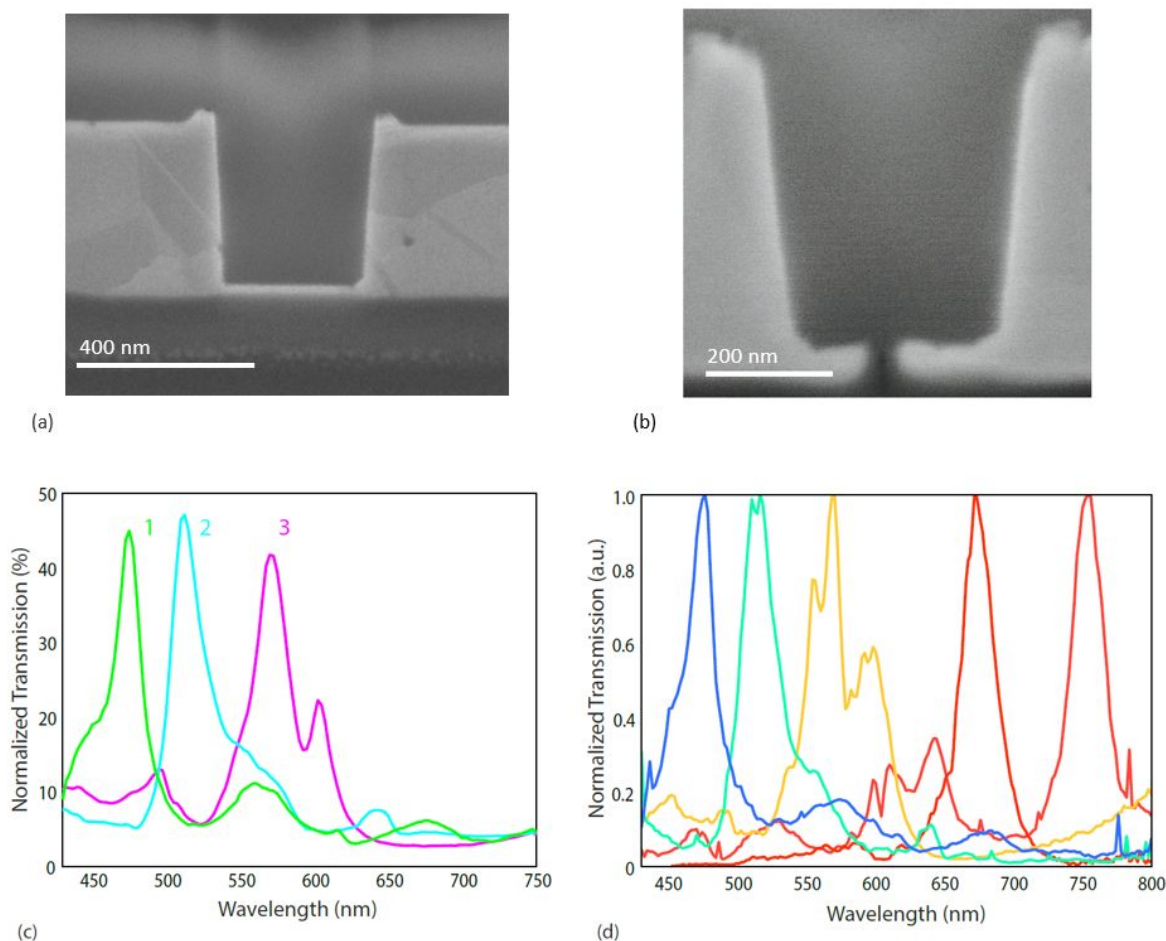


Figure 4 (a) Cross-section of a thinned filter prior to the aligned mill of the slit. (b) Cross-section of a completed filter. The images are both tilted to 52° , exaggerating the apparent taper. The measured tapers of the mirrors of these filters are both less than 3° (c) Measured transmission spectra for 3 linear color filters. Each possesses a FWHM of 31 nm or less and a cross-sectional footprint of less than 600 nm (d) Transmission measurements of 5 linear color filters plotted in the CIE color of their transmission peak. Each filter was normalized to its peak transmission value to emphasize its narrow transmission bandwidth and high signal-to-noise ratio.

The fabricated filters were measured using a supercontinuum laser incident upon a monochromator that is focused through a home-built focusing set-up and a 50X objective to yield a Gaussian beam with a $2\ \mu\text{m}$ spot size. A beam splitter directed some of the incident power to a reference diode that was used to ensure the consistent normalization of all spectra. Multiple filter geometries were measured to verify the spectral response of the simulated filters. Due to the sub-diffraction limit footprint of all filters, they were all normalized relative to $5\ \mu\text{m}$ aperture. This

1
2
3 relatively large aperture was chosen to prevent any resonant effects in the normalization spectrum.
4 If a smaller aperture were used, it would add resonant features into the transmission response that
5 would be convolved with the transmission spectrum of the filter. While the 2 μm beam spot still
6 allowed for the filters to report relatively high transmission efficiencies, these values would be
7 even higher if considered relative to the 1 μm footprint of state-of-the-art CMOS pixels.
8 Normalization was also used to account for the spurious scattered background signal reported by
9 the measurement set-up in the near-IR.
10
11
12
13
14
15

16 Three transmission spectra for different linear color filters are shown in Figure 4(c). The
17 linear filters are polarization dependent and each have a footprint of less than 600 nm in the lateral
18 direction. Filter 1 demonstrated peak transmission at 475.0 nm, indicating that while these filters
19 are made with Ag, they can still perform at wavelengths less than 500 nm. The FWHM of this
20 filter is 24.8 nm, corresponding to a resolving power of 19.2. Filter 2 shows similar behavior at
21 peak position 512.5 nm, FWHM 30.6 nm, and resolving power 16.7. Filter 3's peak at 570.0 had
22 a FWHM and resolving power of 31.5 nm and 18.1 respectively. There is small side-lobe on Filter
23 3, which we suggest is due to a slight misalignment of the filtering slit. Each filter was normalized
24 to a 5 μm square hole through the Ag and reported a normalized transmission of at least 40%,
25 despite the sub-micron width of each slit filter. The footprint of Filter 3 is 0.65 that of Filter 2,
26 which was used as an additional normalization factor to account for the reduced amount of light
27 incident on that filter. Even more importantly, the measured filters demonstrated high signal to
28 noise ratios, indicating that they are well-suited for application in hyperspectral filtering. Figure
29 4(d) illustrates the normalized transmission spectra for filters whose transmission band varies
30 across the visible range. These filters were measured using a transmission confocal set-up with a
31 5 μm circular pinhole aperture (shown in Figure Supplemental Figure 6(c)), which mimics the
32 detection configuration of color filters integrated into CMOS image sensors. In general, the
33 measured filters show excellent agreement with simulation, and the experimental filters possess
34 enhanced transmission that we suggest is due to the very large grain and smooth surfaces of the
35 Ag, which reduces loss within the system²⁴. The experimental filter results validate that the
36 mirrored filter design is capable of breaking the relationship between footprint and resolving power
37 within nanophotonic filters. These filters can produce narrowband transmission spectra with just
38 a single period of the nanophotonic feature.
39
40
41
42
43
44
45
46
47
48
49
50
51
52
53
54
55
56
57
58
59
60

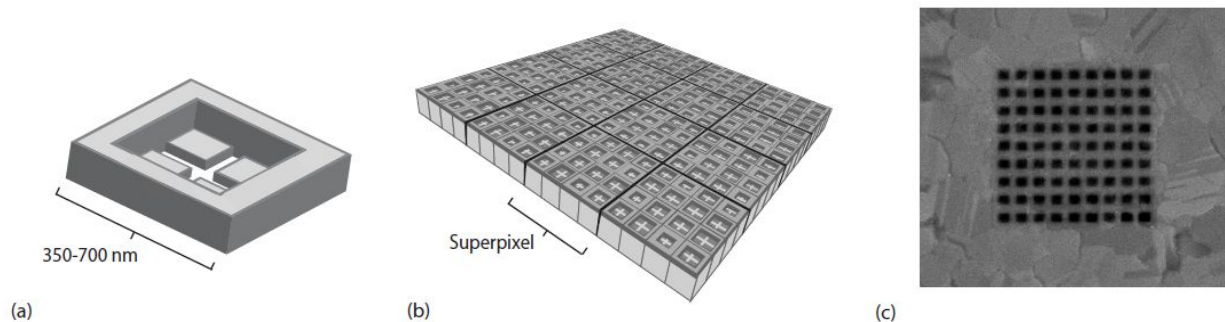


Figure 5 (a) A schematic of a single square filter. The footprint of each side varies from 350 – 700 nm for filters in the visible part of the spectrum. (b) Schematic of a proposed multispectral "superpixel" composed of arrays of ultracompact square filters (c) Electron micrograph of a 9 x 9 array of 424 nm to a side square filters. The dark contrast squares are the SiO₂ pillars between the lighter contrast mirrors. All filters in this array are spaced 200 nm apart.

In a multispectral or hyperspectral image sensor, individual filters are architected in pixel arrays. A potential layout geometry is shown in Figure 5 in which individual square filters (Figure 5(a)) are arrayed into superpixels (Figure 5(b)) that each correspond to a single spatial coordinate, and the filters are all separated by the width of the mirrors that surround the active filtering area. A fabricated array of filters is shown in Figure 5(c). The dark grey squares are the SiO₂ regions between the lighter gray 200 nm wide mirrors. Experimental results for the three-dimensional square filters are shown in Figures 6(a) and 6(b). In 6(a) the transmission results for a single square filter with mirror-to-mirror spacing of 692 nm is shown normalized to a 5 μm aperture. The transmission response demonstrates that a sharp feature can be produced, even for a sub-micron single filter. The noise around the peak is due to fabrication imperfections in individual filters and as can be seen by comparison with spectrally-averaged measurements from multiple square filters, as shown in Figure 6(b), where a 2 x 2 array of the same square filters were measured. Each filter has an edge length of 424 nm and the spacing between the filters is 200 nm. The filters are each spaced less than 200 nm apart and there is no evidence of optical crosstalk between the filters. The leftmost secondary peak is evident in simulations of single pixels of this structure. Slight misalignments of the milled crosses within each filter area is responsible for the slight broadening of this peak, which is less evident in the single filter case. We suggest the other two smaller peaks are also due to these fabrication imperfections. Calculations further demonstrate that not only can same wavelength filters be arrayed close together, so can filters targeting different wavelengths. Figure 6(c) illustrates an array of simulations where the spacing between two adjacent filters was

varied from 10 nm to 70 nm. The two peaks at 612.2 and 718.1 nm correspond to the transmission bands of the individual filters. Once the spacing between the filters exceeds the skin depth of Ag, 50 nm at these wavelengths, there is no evidence of optical crosstalk between the filters. This indicates that in a device, filters can be spaced as close as 50 nm apart without introducing artifacts from optical crosstalk.

By coupling an in-plane Fabry-Perot resonator to a surface plasmon polariton mode, and

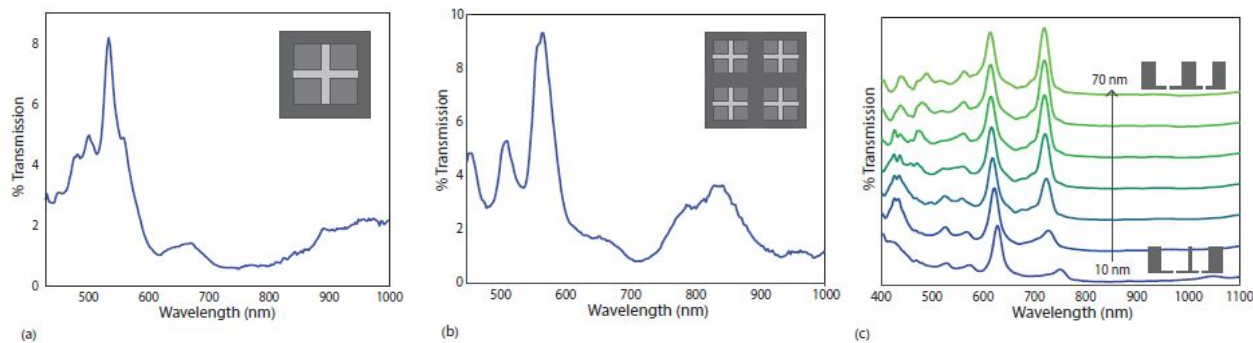


Figure 6 (a) Transmission spectrum for a single square filter that has an edge-length of 692 nm (b) Transmission spectrum for a 2 x 2 array of square filters. Each filter has edge-lengths of 424 nm and they are spaced 200 nm apart. The single narrow peak experimentally verifies that square filters produce the expected response and arrays of pixels do not possess optical crosstalk (c) Calculated crosstalk between two spectrally distinct linear filters. The width of the mirror separating the two active filter areas varies from 10 nm (blue) to 70 nm (green). There is no evidence of optical crosstalk in filters spaced at least 50 nm apart.

utilizing a novel metal imprint fabrication method for filter fabrication, we were able to design ultracompact narrowband transmission color filters that break the relationship between footprint and resolving power. Filters were experimentally shown to achieve narrowband spectral filtering and function in pixel arrays. The filtering mechanism is not dependent on any absolute length scale, so larger filters can be used to filter longer wavelength light utilizing Ag or other materials systems. For example, filters employing Cu mirrors have been shown to be extremely effective at filtering light in the near-IR part of the spectrum, as shown in Supplemental Figure S7. Additionally, while these filters are static, introducing a gate-tunable dielectric like ITO could potentially be used to spectrally tune the peak transmission wavelength, and thus reduce the number of filters needed to form a superpixel without reducing the spectral resolution.

Methods

1
2
3 *Optimization Method:* The process for optimizing the filter structure using the NOMAD algorithm
4 and this FOM (main text, Eqn. 1) is illustrated in Supplemental Figure 3. All steps are performed
5 automatically after the optimization process is initiated, using the optimization defaults unless
6 indicated in Supplementary Table 2. In this method, the algorithm suggests a set of physical
7 parameters for the filter. Lumerical Finite Difference Time Domain simulation package (FDTD),
8 and eigenmode solver, then uses these parameters to perform a simulation to determine the filter's
9 optical response. The resulting transmission spectrum of the filter is then analyzed by a custom
10 peak-finding algorithm, which was developed to include both the maxima at the edges of a vector
11 and plateaus, to make sure that all peak-like features would be properly identified and accounted
12 for. Using the analyzed spectrum, the FOM is calculated, and used by NOMAD to suggest a new
13 set of physical parameters. This process repeats until the convergence criteria is met.
14
15
16
17
18
19
20
21
22
23

24 *Fabrication Method:* The sidewalls of the mirrors closely control the transmission behavior of the
25 filters. Slight changes to the mirror spacing or taper can dramatically change filter performance.
26 To closely control the quality of the mirrors, the filters were fabricated using a metal-imprinting
27 process. This method, shown in Supplemental Figure 4 produces mirrors with straighter sidewalls
28 than lift-off processing with the added benefit of producing extremely smooth metal structures.
29
30
31
32
33

34 The fabrication method is discussed in detail in the Supplemental Information and a schematic of
35 the process flow is provided in Supplemental Figure 4. The method consists of four main initial
36 steps: defining the SiO₂ structures that form the negative space around the metal mirrors using
37 electron beam lithography and dry etching, infilling the Ag mirrors with electron beam deposition
38 and a metal imprinting process, removing excess Ag and smoothing the remaining metal with a
39 dry etch and the imprinting method, then etching the slit in the metal film and encapsulating with
40 insulating materials.
41
42
43
44
45
46
47

48 *Measurement Set-up and Analysis:* Transmission measurements were performed with a custom-
49 built optical set-up that uses an NKT SuperK Extreme white laser as the light source. As shown in
50 Supplemental Figure 6, the beam was monochromated with variable slit width to give a constant
51 bandpass of 2nm, collimated, expanded by two 90 degree off-axis parabolic mirrors, and finally
52 focused onto the sample with a long working distance, low-NA objective (Mitutoyo Plan Apo 50X,
53
54
55
56
57
58
59
60

1
2
3 Tube Length 200mm, NA=0.55). A CMOS (IDS UI-1460SE) camera was used to experimentally
4 characterized the beam shape at the focal plane and verified it had a FWHM of ~2nm. The set-up
5 was used in this configuration to perform the measurements of the linear filters shown in Figures
6 4(c) and the crossed filters shown in Figure 6.
7
8
9

10 To confirm there were no artifacts from background signal present in these measurements,
11 the background signal needed to be further attenuated so the above set-up was modified into a
12 transmission confocal microscopy configuration. The same monochromatic and collimated beam
13 was redirected 180° via mirrors to enter the objective passing through its focal point. A second
14 objective, pinhole, and low dark current photodiode were incorporated into the beam path to
15 perform these measurements. Peak normalized signal-to-noise (SNR) plots were created using
16 this method because it significantly increased spatial signal contrast and greatly reduced the
17 background spectrum such that sub-percent peaks could be detected without a loss in SNR. The
18 normalization spectrum for each filter was measured on an area of the fused silica superstrate
19 where no Ag film existed, which accounted for the reflection of the superstrate. The specific
20 method for calibration and the details for the remaining components in the optical beam path are
21 described in detail in the Supplemental Information.
22
23
24
25
26
27
28
29
30
31
32
33
34
35
36
37
38
39
40
41
42
43
44
45
46
47
48
49
50
51
52
53
54

55 **Acknowledgments**

56
57
58
59
60

This work was supported by the Air Force Office of Scientific Research under grant number FA9550-16-1-0019. G.T. acknowledges support from the Swiss National Science Foundation through the Advanced Mobility Fellowship, Grant P300P2_171417. D.F. gratefully acknowledges Artur Davoyan, Matt Sullivan Hunt, Michelle Sherrott, Phil Jahelka and Sisir Yalamanchili for useful discussions during the development of this work.

Author Contributions

D.F. and H.A.A. conceived of the ideas. K.F. formatted the optimization code, built the peak finding algorithm, and designed the FOM with input from D.F. D.F. used the optimization code to identify the filter geometry. D.F. developed the fabrication method and made the filters. G.T. and C.B. built the measurement set-up. D.F. and C.B. took the measurements and G.T. contributed to data analysis. D.F. and H.A.A. co-wrote the paper. All authors discussed the results and commented on the manuscript, and H.A.A. supervised.

Competing financial interests

The authors declare no competing financial interests.

Data Availability

The data that support the findings of this study are available from the corresponding author upon reasonable request.

Supporting Information

Additional information about the nature of the behavior of the transmission color filters, the optimization method, the fabrication method, and the measurement set-up and analysis is available in the Supplemental Information. This material is available free of charge via the Internet at <http://pubs.acs.org>

References

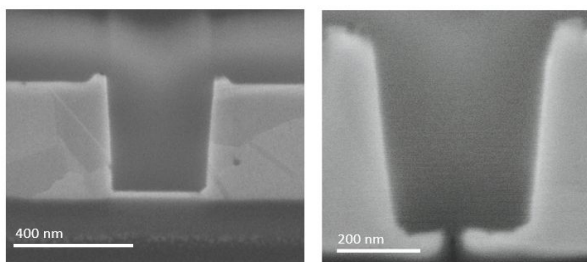
- (1) Moore, G. E. Cramming More Components onto Integrated Circuits. *Proc. IEEE* **1965**, *86*, 82–85.
- (2) Thompson, D. A.; Best, J. S. The Future of Magnetic Data Storage Technology. *IBM J. Res. Dev.* **2000**, *44*, 311–322. <https://doi.org/10.1147/rd.443.0311>.
- (3) Hecht, J. Is Keck's Law Coming to an End. *IEEE Spectr.* **2016**, 11–23.
- (4) Horie, Y.; Han, S.; Lee, J.-Y.; Kim, J.; Kim, Y.; Arbabi, A.; Shin, C.; Shi, L.; Arbabi, E.; Kamali, S. M.; et al. Visible Wavelength Color Filters Using Dielectric Subwavelength Gratings for Backside-Illuminated CMOS Image Sensor Technologies. *Nano Lett.* **2017**, *17*, 3159–3164.
- (5) Yokogawa, S.; Burgos, S. P.; Atwater, H. A. Plasmonic Color Filters for CMOS Image Sensor Applications. *Nano Lett.* **2012**, *12*, 4349–4354. <https://doi.org/10.1021/nl302110z>.
- (6) Chen, Q.; Hu, X.; Wen, L.; Yu, Y.; Cumming, D. R. S. Nanophotonic Image Sensors. *Small.* **2016**, pp 4922–4935. <https://doi.org/10.1002/sml.201600528>.
- (7) Jang, W.-Y.; Ku, Z.; Jeon, J.; Kim, J. O.; Lee, S. J.; Park, J.; Noyola, M. J.; Urbas, A. Experimental Demonstration of Adaptive Infrared Multispectral Imaging Using Plasmonic Filter Array. **2016**, *6*, 34876.
- (8) Yudovsky, D.; Nouvong, A.; Pilon, L. *Hyperspectral Imaging in Diabetic Foot Wound Care*. SAGE Publications Sage CA: Los Angeles, CA 2010.

- 1
2
3
4
5
6
7
8
9
10
11
12
13
14
15
16
17
18
19
20
21
22
23
24
25
26
27
28
29
30
31
32
33
34
35
36
37
38
39
40
41
42
43
44
45
46
47
48
49
50
51
52
53
54
55
56
57
58
59
60
- (9) Gowen, A. A.; O'Donnell, C. P.; Cullen, P. J.; Downey, G.; Frias, J. M. Hyperspectral Imaging – an Emerging Process Analytical Tool for Food Quality and Safety Control. *Trends Food Sci. Technol.* **2007**, *18*, 590–598. <https://doi.org/10.1016/j.tifs.2007.06.001>.
 - (10) Hege, E. K.; O'Connell, D.; Johnson, W.; Bastly, S.; Dereniak, E. L. Hyperspectral Imaging for Astronomy and Space Surveillance. *Opt. Sci. Technol. SPIE's 48th Annu. Meet.* **2004**, *5159*, 380–391. <https://doi.org/10.1117/12.506426>.
 - (11) Fleischman, D.; Sweatlock, L. A.; Murakami, H.; Atwater, H. Hyper-Selective Plasmonic Color Filters. *Opt. Express* **2017**, *25*, 27386–27395.
 - (12) Wang, S. S.; Magnusson, R. Theory and Applications of Guided-Mode Resonance Filters. *Appl. Opt.* **1993**, *32* (14), 2606–2613. <https://doi.org/10.1364/AO.32.002606>.
 - (13) Mazulquim, D. B.; Lee, K. J.; Yoon, J. W.; Muniz, L. V.; Borges, B.-H. V.; Neto, L. G.; Magnusson, R. Efficient Band-Pass Color Filters Enabled by Resonant Modes and Plasmons near the Rayleigh Anomaly. *Opt. Express* **2014**, *22*, 30843–30851. <https://doi.org/10.1364/OE.22.030843>.
 - (14) Macleod, H. A.; Macleod, H. A. *Thin-Film Optical Filters*; CRC press, 2010.
 - (15) Grepstad, J. O.; Greve, M. M.; Holst, B.; Johansen, I.-R.; Solgaard, O.; Sudbø, A. Finite-Size Limitations on Quality Factor of Guided Resonance Modes in 2d Photonic Crystals. *Opt. Express* **2013**, *21*, 23640–23654.
 - (16) Yoon, Y.-T.; Lee, S.-S. Transmission Type Color Filter Incorporating a Silver Film Based Etalon. *Opt. Express* **2010**, *18*, 5344–5349.
 - (17) Zeng, B.; Gao, Y.; Bartoli, F. J. Ultrathin Nanostructured Metals for Highly Transmissive Plasmonic Subtractive Color Filters. *Sci. Rep.* **2013**, *3*, 2840.
 - (18) Čtyroký, J.; Gonzalo Wangüemert-Pérez, J.; Kwiecien, P.; Richter, I.; Litvik, J.; Schmid, J. H.; Molina-Fernández, Í.; Ortega-Moñux, A.; Dado, M.; Cheben, P. Design of Narrowband Bragg Spectral Filters in Subwavelength Grating Metamaterial Waveguides. *Opt. Express* **2018**, *26*, 179. <https://doi.org/10.1364/OE.26.000179>.
 - (19) Barton, J. H.; Rumpf, R. C.; Smith, R. W.; Kozikowski, C. L.; Zellner, P. A. All-Dielectric Frequency Selective Surfaces with Few Number of Periods. *Prog. Electromagn. Res.* **2012**, *41*, 269–283.
 - (20) Rios, L. M.; Sahinidis, N. V. Derivative-Free Optimization: A Review of Algorithms and Comparison of Software Implementations. *J. Glob. Optim.* **2013**, *56*, 1247–1293.
 - (21) Audet, C.; J. E. Dennis, J. Mesh Adaptive Direct Search Algorithms for Constrained Optimization. *SIAM J. Optim.* **2006**, *17*, 188–217.
 - (22) Le Digabel, S. Algorithm 909: NOMAD: Nonlinear Optimization with the MADS Algorithm. *ACM Trans. Math. Softw.* **2011**, *37*, 44:1--44:15.
 - (23) Park, J. H.; Nagpal, P.; McPeak, K. M.; Lindquist, N. C.; Oh, S.-H.; Norris, D. J. Fabrication of Smooth Patterned Structures of Refractory Metals, Semiconductors, and Oxides via Template Stripping. *ACS Appl. Mater. Interfaces* **2013**, *5*, 9701–9708.
 - (24) McPeak, K. M.; Jayanti, S. V.; Kress, S. J. P.; Meyer, S.; Iotti, S.; Rossinelli, A.; Norris, D. J. Plasmonic Films Can Easily Be Better: Rules and Recipes. *ACS photonics* **2015**, *2*, 326–333.

1
2
3
4 For Table of Contents Use Only
5

6 Title: High Spectral Resolution Plasmonic Color Filters with Subwavelength Dimensions
7

8
9 Authors: Dagny Fleischman, Katherine T. Fountaine, Colton R. Bukowsky, Giulia Tagliabue,
10 Luke A. Sweatlock, and Harry A. Atwater
11



24 Cross-sectional SEM micrographs of a narrowband transmission color filters with dimensions
25 determined using inverse design. Filters were fabricated using a novel metal imprinting method
26 that produced metallic nanostructures with extremely smooth surfaces, which enabled the
27 demonstration of high spectral resolution color filtering with a smaller footprint than any
28
29 previously reported.
30
31
32
33
34
35
36
37
38
39
40
41
42
43
44
45
46
47
48
49
50
51
52
53
54
55
56
57
58
59
60